

# Pair-Production Supernovae: Theory and Observation

By **Evan Scannapieco**<sup>1</sup>

<sup>1</sup>Kavli Institute for Theoretical Physics, Kohn Hall, UC Santa Barbara, Santa Barbara, CA 93106

Nonrotating stars that end their lives with masses  $140 M_{\odot} \leq M_{\star} \leq 260 M_{\odot}$  should explode as pair-production supernovae (PPSNe). Here I review the physical properties of these objects as well as the prospects for them to be constrained observationally.

In very massive stars, much of the pressure support comes from the radiation field, meaning that they are loosely bound, and that  $(d \lg p / d \lg \rho)_{\text{adiabatic}}$  near the center is close to the minimum value necessary for stability. Near the end of *C/O* burning, the central temperature increases to the point that photons begin to be converted into electron-positron pairs, softening the equation of state below this critical value. The result is a runaway collapse, followed by explosive burning that completely obliterates the loosely-bound star. While these explosions can be up to 100 times more energetic than core collapse and Type Ia supernovae, their peak luminosities are only slightly greater. However, due both to copious  $\text{Ni}^{56}$  production and hydrogen recombination, they are brighter much longer, and remain observable for  $\approx 1$  year.

Since metal enrichment is a local process, PPSNe should occur in pockets of metal-free gas over a broad range of redshifts, greatly enhancing their detectability, and distributing their nucleosynthetic products about the Milky Way. This means that measurements of the abundances of metal-free stars should be thought of as directly constraining these objects. It also means that ongoing supernova searches, which limit the contribution of very massive stars to  $\lesssim 1\%$  of the total star formation rate density out to  $z \approx 2$ , already provide weak constraints for PPSN models. A survey with the NIRCcam instrument on JWST, on the other hand, would be able to extend these limits to  $z \approx 10$ . Observing a  $0.3 \text{ deg}^2$  patch of sky for  $\approx 1$  week per year for three consecutive years, such a program would either detect or rule out the existence of these remarkable objects.

---

## 1. Introduction

Pair-production supernovae (PPSNe) are the uniquely calculable result of nonrotating stars that end their lives in the  $140 - 260 M_{\odot}$  mass range (Heger & Woosley 2002, hereafter HW02). Their collapse and explosion result from an instability that generally occurs whenever the central temperature and density of star moves within a well-defined regime (Barkat, Rakavy, & Sack 1967). While this instability arises irrespective of the metallicity of the progenitor star, PPSNe are expected only in primordial environment, and there are three main reasons for this association.

Firstly, in the present metal-rich universe, it appears that stars this large are never assembled, as supported by a wide range of observations. Figer (2005) carried out a detailed study of the  $Z \approx Z_{\odot}$  Arches cluster, which is large ( $M_{\star} > 10^4 M_{\odot}$ ), young ( $\tau = 2.0 - 2.5$  Myrs), and at a well-determined distance, making it ideal for such studies. No stars more massive than  $130 M_{\odot}$  were found, although more than 18 were expected. A similar  $\approx 150 M_{\odot}$  limit was found in the lower metallicity cluster R136 in the Large Magellanic Cloud (Weidener & Kroupa 2003), and from a grab-bag of clusters compiled by Oey & Clarke (2005).

However, there are good theoretical reasons to believe that the situation may have been very different under primordial conditions. In this case the primary coolant at low temperatures is molecular hydrogen, which starts to be populated according to local

thermodynamic equilibrium (LTE) at a typical density and temperature of  $\approx 10^4 \text{ cm}^{-3}$  and 100 K. As the Jeans mass under these conditions is  $\approx 10^3 M_\odot$  the fragmentation of primordial molecular clouds may have been biased towards the formation of stars with very high masses (Nakamura & Umemura 1999; Abel Bryan & Norman 2000, Schneider et al. 2002; Tan & McKee 2004).

Finally, as very massive, radiatively supported stars are only loosely bound they tend to drive large winds. However, these winds are primarily line-driven and scale with metallicity as  $Z^{1/2}$  or faster (Kudritzki 2000; Vink et al. 2001; Kudritzki 2002). As long as another mechanism did not act to generate significant mass loss in primordial stars (e.g. Smith & Owocki 2006) this raises the real possibility that they may have not only been born, but have ended the lives in the mass range necessary to drive PPSNe.

This conference proceeding summarizes both the underlying physics and the prospects for observation of these most powerful of astrophysical explosions, and it is structured as follows: In §2 I describe the pair-production instability in detail, and how it eventually leads to stellar disruption. In §3 I discuss the post-explosion physics of these objects, and how it effects their luminosity and temperature evolution. In §4 I discuss the optical light-curves of PPSNe, and contrast them with lightcuves of SNe Type-II and Ia. §5 discusses the redshift evolution of metal-free stars, and its implications for PPSN environments. In §6 these estimates are used to determine the feasibility of present and future PPSN. In §7 and §8 I discuss the likely distribution of the descendents of metal-free stars in the Galaxy, and I close with a short summary in §9.

## 2. Physics of Pair-Production Supernovae

The instability that leads to the formation of PPSNe was first identified by Barkat, Rakavy, & Sack (1967), who carried out a detailed analysis of the relevant equation of state for very massive stars near the end of their lifetimes. These results are shown in Figure 1. In hydrostatic balance  $p \propto M^{2/3} \rho^{4/3}$ , which means that if the adiabatic coefficient softens to below  $\gamma = 4/3$ , the star will become unstable to runaway collapse.

Figure 1 shows that such a collapse occurs for stars with central temperatures from  $10^9$  to  $3 \times 10^9$ , and central densities less than  $5 \times 10^5 \text{ g cm}^{-3}$ . This region is bounded by three limits. Below the low-temperature boundary on the left, most of the central pressure is provided by the radiation field, such that  $\gamma \approx 4/3$ . As the temperature increases, photon energies rise to the point that electron-positron pairs begin to be made, removing energy from the radiation field and softening  $\gamma$  below the critical value. The high-density end of this region, on the other hand, is bounded by degeneracy pressure, which provides sufficient support to halt collapse at high densities. Finally, at the high temperature boundary of the pair-instability regime, the energy consumed in creating the rest mass becomes less significant, and  $\gamma$  remains above  $4/3$ .

As massive stars are very loosely bound, their evolution is somewhat more complicated than their lower mass counterparts, and thus requires more detailed numerical modeling. As stars with masses above  $140 M_\odot$  collapse, their central temperature and density quickly increases, moving right through the unstable regime and starting explosive burning in the carbon-oxygen core. This explosive burning takes place in an environment in which there are very few excess neutrons, which results in a large deficiency in the number of nuclei with odd charge above  $^{14}\text{N}$ . Thus elements such as Na, Al, and P are almost 2 orders of magnitude less abundant than neighboring element with even charge such as Ne, Mg, and Si. This strong “odd-even effect” is a very general feature that is unavoidable in a model of the nucleosynthetic products of PPSNe (HW02).

Models of the kinematics of PPSNe are similarly robust. For stars with initial masses

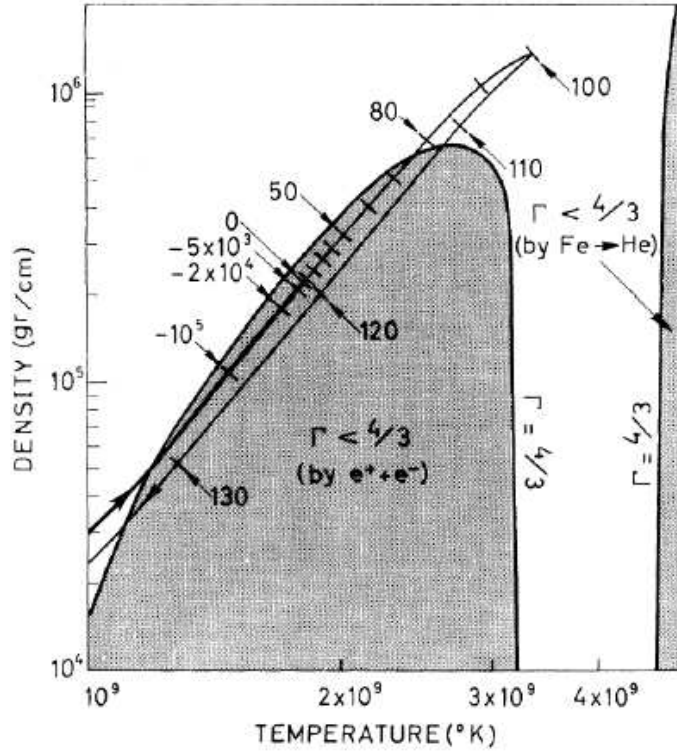


FIGURE 1. Original plot from Barkat, Rakavy, & Sack (1967) showing the range of central temperatures and densities at which the equation of state softens below the  $\gamma = 4/3$  value required for stability. The solid lines give an early estimate of the evolution of a star with a  $40 M_{\odot}$  oxygen core near the end of its life. Finally the region on the right shows the temperature and density region relevant in usual core-collapse supernovae.

more than about  $140 M_{\odot}$ , the energy released during explosive burning is sufficient to completely disrupt the star, resulting in a PPSN. This complete disruption means that while the evolution of these stars is somewhat more complex than lower mass stars, the explosion mechanism driving the resulting supernovae is far simpler. There are no issues of fallback, mass-cut, or neutrino heating, and in the nonrotating case, the results are uniquely calculable.

A shock moves outward from the edge of the core, initiating the supernova outburst when it reaches the stellar surface. Just above the  $140 M_{\odot}$  limit, weak silicon burning occurs and only trace amounts of radioactive  $^{56}\text{Ni}$  are produced and it is this  $^{56}\text{Ni}$  that powers the late-time supernova light curves. The amount of  $^{56}\text{Ni}$  produced increases in larger progenitors, and in  $260 M_{\odot}$  progenitors up to  $50 M_{\odot}$  may be synthesized,  $\approx 100$  times more than in a typical Type Ia supernova. For stars with masses above  $260 M_{\odot}$ , however, the onset of photodisintegration in the center imposes an additional instability that collapses most of the star into a black hole (Bond, Arnett & Carr 1984; HW02; Fryer, Woosley, & Heger 2001).

Pair-production supernovae are among most powerful thermonuclear explosions in the universe, with a total energies ranging from  $3 \times 10^{51}$  ergs for a  $140 M_{\odot}$  star ( $64 M_{\odot}$  helium  $M_{\odot}$  core) to almost  $100 \times 10^{51}$  ergs for a  $260 M_{\odot}$  star ( $133 M_{\odot}$  helium core; HW02). In Scannapieco et al. (2005, hereafter S05), we used the implicit hydrodynamical code KE-

TABLE 1. Properties of PPSN progenitor models

Model	$M_{\text{He}}$ ( $M_{\odot}$ )	$M_{\text{N}}$ ( $M_{\odot}$ )	$M_{^{56}\text{Ni}}$ ( $M_{\odot}$ )	$R$ ( $10^{13}$ cm)	$\mathcal{E}_{\text{kin}}$ ( $10^{51}$ ergs)
150-W	70	3.5(-4)	4.2(-2)	3.9	6.9
150-I	46	1.1(-4)	6.3(-2)	16	9.2
150-S	49	0.86	8.6(-2)	26	8.5
200-W	97	2.7(-6)	3.3	0.68	29.5
200-I	58	8.0(-6)	5.1	2.8	36.5
200-S	89	0.34	2.2	29	29.1
200-S2	78	4.75	0.82	20	18.7
250-W	123	3.1(-6)	6.2	0.58	47.2
250-I	126	9.1(-6)	32	4.0	76.7
250-S	113	1.34	24.5	26	64.6

PLER (Weaver, Zimmerman, & Woosley 1978) to model the entire evolution of the star and the resulting light curves. KEPLER implements gray diffusive radiation transport with approximate deposition of energy by gamma rays from radioactive decay of  $^{56}\text{Ni}$  and  $^{56}\text{Co}$  (Eastman et al. 1993), and the light curves obtained can only be followed as long as there is a reasonably well-defined photosphere.

A supernova can be bright either because it makes a lot of radioactive  $^{56}\text{Ni}$  (as in Type Ia supernovae) or because it has a large low density envelope and large radius (as in bright Type II supernovae). More radioactivity gives more energy at late times, while a larger initial radius results in a higher luminosity at early times. Here, the most important factors in determining the resulting light curves are the mass of the progenitor star and the efficiency of dredge-up of carbon from the core into the hydrogen envelope during or at the end of central helium burning. The specifics of the physical process encountered here are unique to primordial stars. Lacking initial metals, they have to produce the material for the CNO cycle themselves, through the synthesis of  $^{12}\text{C}$  by the triple-alpha process. Just enough  $^{12}\text{C}$  is produced to initiate the CNO cycle and bring it into equilibrium: a mass fraction of  $10^{-9}$  when central hydrogen burning starts, and a mass fraction  $\sim 10^{-7}$  during hydrogen-shell burning.

At these low values, the entropy in the hydrogen shell remains barely above that of the core, and the steep entropy gradient at the upper edge of the helium core that is typical for metal-enriched helium-burning stars is absent. This means that, during helium burning the central convection zone can get close, nip at, or even penetrate the hydrogen-rich layers. Once such mixing of high-temperature hydrogen and carbon occurs, the two components burn violently, and even without this rapid reaction, the hydrogen burning in the CNO cycle increases proportionately to the additional carbon. Thus mixing of material from the helium-burning core, which has a carbon abundance of order unity, is able to raise the energy generation rate in the hydrogen-burning shell by orders of magnitude over its intrinsic value.

This mixing has two major effects on the PPSN progenitor: first, it increases the opacity and energy generation in the envelope, leading to a red-giant structure for the presupernova star, in which the radius increases by over an order of magnitude. Second, it decreases the mass of the He core, consequently leading to a smaller mass of  $^{56}\text{Ni}$  being synthesized and a smaller explosion energy. The former effect increases the luminosity of the supernova, at early times, while the latter effect can weaken it, and in S05 we accounted for these uncertainties by employing different values of convective overshooting.

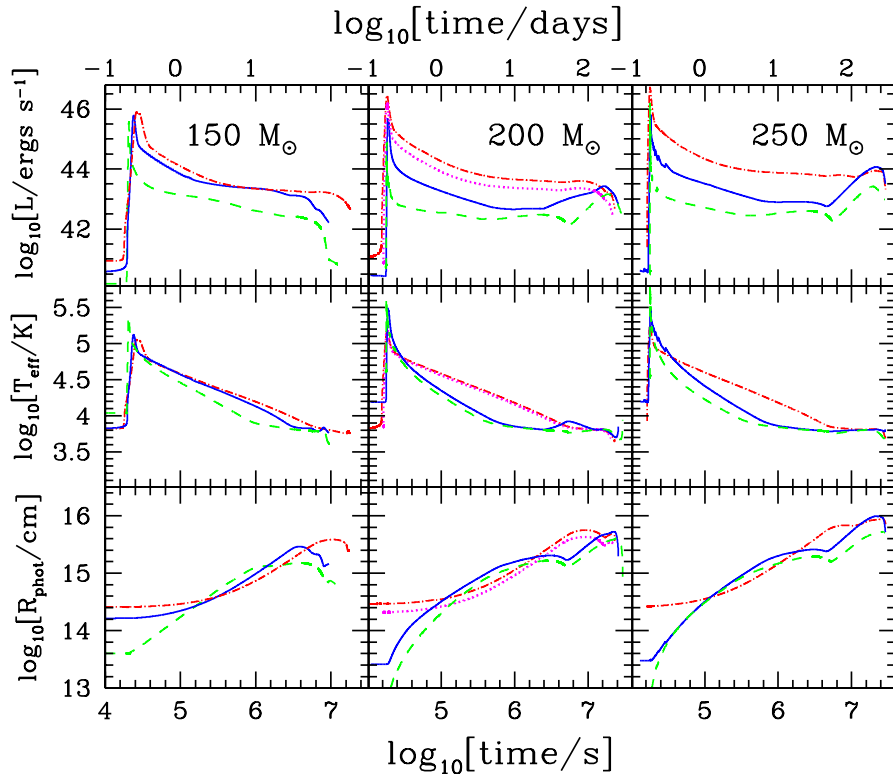


FIGURE 2. Luminosities (top row), effective temperatures (center row), and photospheric radii (bottom row) of PPSNe for ten different representative models. Each sets of panels are labeled by the total mass of the progenitor star, and models with weak (dashed), intermediate (solid) and strong (dot-dashed) convective overshoot are shown. Finally, the dotted lines in the central panels correspond to model 200-S2. See text and Table 1 for details.

A suite of representative models was chosen to address the expected range of presupernova models - from blue supergiant progenitors with little or no mixing to well-mixed red hypergiants, which can have pre-SN radii of 20 AU or more. These models are summarized in Table 1, in which the names refer to the mass of the progenitor star (in units of  $M_{\odot}$ ) and the weak (W), intermediate (I), or strong (S) level of convective overshoot. Here we show the final mass in helium, nitrogen, nickel, the radius just before the explosion, and the kinetic energy of the explosion in units of  $10^{51}$  ergs.

### 3. Luminosity and Temperature Evolution

The KEPLER code can be used to compute approximate light curves and has been validated both against much more complex and realistic codes such as EDDINGTON and observations of a prototypical Type II-P supernova, SN 1969L (Weaver and Woosley 1980; Eastman et al 1994), although its main deficiency is that it is a single temperature code using flux-limited radiative diffusion. The evolution of the luminosities, effective temperatures, and photospheric radii for the models in Table 1, are shown in Figure 2.

As the shock moves toward the low-density stellar surface, its energy is deposited into progressively smaller amounts of matter. This results in high velocities and temperatures when the shock reaches the stellar surface, causing a pulse of ultraviolet radiation with a characteristic timescale of a few minutes. This “breakout” phase is by far the most luminous and bluest phase of the PPSN burst, but its very short duration makes it difficult to use in observational searches. In fact, the analog of this phase in conventional SNe has so far only been indirectly detected in SN 1987A (e.g. Hamuy et al. 1988; Catchpole et al. 1988).

Following breakout, the star expands with  $R_{\text{phot}}$  initially proportional to time. Though a small fraction of the outer mass may move much faster, the characteristic velocity of the photosphere during this phase is a modest  $v = (2KE/M)^{1/2} \sim (10^{53}\text{ergs}/200 M_{\odot})^{1/2} \sim 5000$  km/s, because of the very large mass participating in the explosion. During the expansion, the radiation-dominated ejecta cool adiabatically, with  $T$  approximately proportional to  $R^{-1}$ , with an additional energy input from the decay of  $^{56}\text{Ni}$  (if a significant mass was synthesized during the explosion) and hydrogen recombinations (when  $T \approx 10^4\text{K}$ ). As the scale radius for this cooling is the radius of the progenitor, the temperatures and luminosities are substantially larger throughout this phase in the cases with the strongest mixing.

After  $\approx 50$  days, the energy input from  $^{56}\text{Co}$  decay becomes larger than the remaining thermal energy and the energy deposited by  $^{56}\text{Co}$  in deeper layers that were enriched in  $^{56}\text{Ni}$  can diffuse out. For stars that were compact to begin with, this can cause a delayed rise to the peak of the light curve. For stars with larger radii, the radioactivity just makes a bright tail following the long plateau in emission from the expanding envelope. Eventually, even the slow-moving inner layers recombine and there is no longer a well-defined photosphere. At this time the assumption of LTE breaks down, and more detailed radiative transfer calculations are required, which are beyond the scope of our S05 modeling. The SN is fainter and redder during this phase, however, and thus is difficult to detect at cosmological distances in optical and near infrared (NIR) surveys.

#### 4. PPSNe Lightcurves

In S05, we calculated approximate PPSNe lightcurves, assuming a black body distribution with the color temperature equal to the effective temperature. Recall that the peak frequency in this case occurs at a wavelength of  $5100(T_{\text{eff}}/10000\text{K})^{-1}$  Å. The resulting light curves are shown in Figure 3 which gives the evolution of AB magnitudes at three representative wavelengths: 5500 Å, corresponding to the central wavelength of the V-band; 4400 Å, corresponding to the B-band; and 3650 Å, corresponding to the U-band. We focus on blue wavelengths as it is features in these bands that will be redshifted into the optical and NIR at cosmological distances. For comparison, we also include observed light curves for a SN Type Ia (1994D as measured by Patat et al. 1996 and Cappellaro et al. 1997) a SN Type II-P (1999em as observed by Elmhamdi et al. 2003), and the very bright Type II-L SN 1979C (de Vaucouleurs et al. 1981; Barbon et al. 1982).

The most striking feature from this comparison is that despite enormous kinetic energies of  $\sim 50 \times 10^{51}$  ergs, the peak optical luminosities of PPSNe are similar to those of other SNe, even falling below the Ia and II curves in many cases. This is because the higher ejecta mass produces a large optical depth and most of the internal energy of the gas is converted into kinetic energy by adiabatic expansion. Furthermore, the colors of the PPSN curves are not unlike those of more usual cases. In fact, pair-production supernovae spend most of their lives in the same temperature range as other SNe. Clearly,

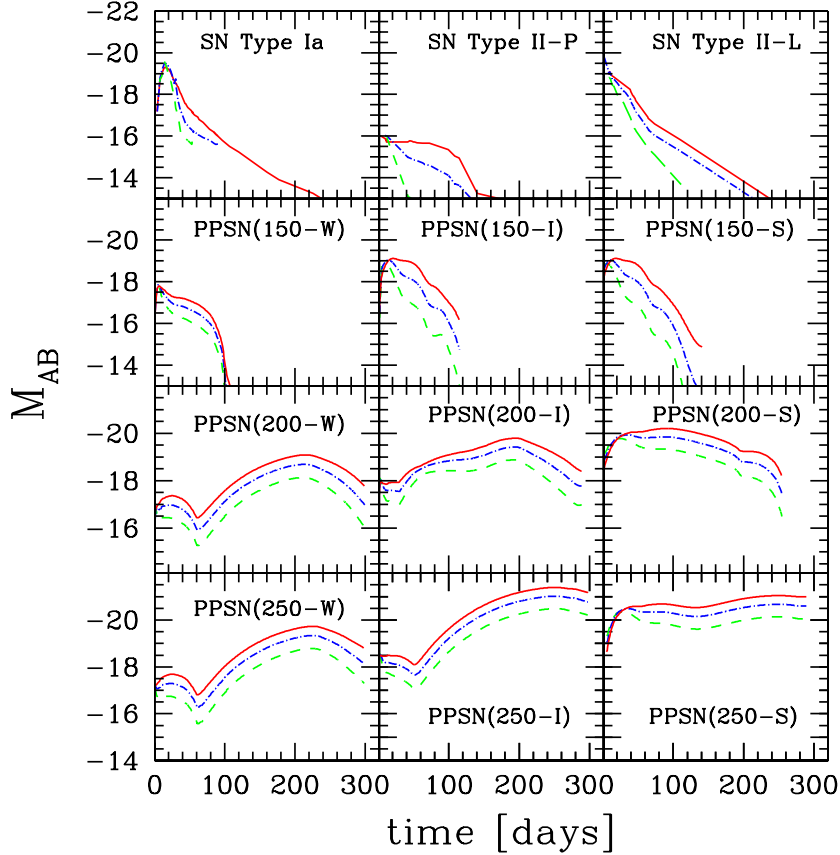


FIGURE 3. Comparison of light curves of a SN Type Ia, a SN Type II-P, a bright SN Type II-L, and PPSNe models with varying progenitor masses and levels of dredge-up. In all cases the solid lines are absolute V-band AB magnitudes, the dot-dashed lines are the absolute B-band AB magnitudes, and the dashed lines are the absolute U-band AB magnitudes.

then, PPSNe will not be obviously distinguishable from their more usual counterparts “at first glance.”

Rather, distinguishing PPSNe will from other SNe will require multiple observations that constrain the time evolution of these objects. In particular there are two key features that are uniquely characteristic to PPSNe. The first of these is a dramatically extended intrinsic decay time, which is especially noticeable in the models with the strongest enrichment of CNO in the envelope. This is due to the long adiabatic cooling times of supergiant progenitors, whose radii are  $\sim 20$  AU, but whose expansion velocities are similar or even less than those of other SNe. Second, PPSNe are the only objects that show an extremely late rise at times  $\geq 100$  days. This is due to energy released by the decay of  $^{56}\text{Co}$ , which unlike in the Type Ia case, takes months to dominate over the internal energy imparted by the initial shock. In this case the feature is strongest in models with the least mixing and envelope enrichment during helium burning, as these have the largest helium cores and consequently the largest  $^{56}\text{Ni}$  masses.

Note, however, that neither of these features is generically present in all PPSNe, and both can be absent in smaller VMS that fail expand to large sizes through dredge-up and do not synthesize appreciable amounts of  $^{56}\text{Ni}$ . In the 150-W case, for example, the luminosity decays monotonically on a relatively short time scale, producing a lightcurve similar to the comparison Type II curves. In fact this 150  $M_{\odot}$  SN shares many features with its smaller-mass cousin: both are SNe from progenitors with radii  $\sim 10^{13}$  cm and in both  $^{56}\text{Ni}$  plays a negligible role. In no case, however, do PPSNe look anything like SNe Type Ia. In particular none of the pair-production models display the long exponential decay seen in the Type Ia curves, and all PPSNe contain hydrogen lines, arising from their substantial envelopes.

## 5. The Redshift Evolution of Metal-Free Stars

Planning searches for PPSNe not only depends on understanding their lightcurves, but also the environments and redshifts at which they are most likely to be located. In Scannapieco, Schneider, & Ferrara, (2003; hereafter SSF03) we showed that cosmological enrichment is a local process, such that the transition from metal-free to Population II stars is heavily dependent on the efficiency with which metals were mixed into the intergalactic medium. This efficiency depends in turn on the kinetic energy input from PPSNe, which was parameterized by the “energy input per unit primordial gas mass”  $\mathcal{E}_g^{III}$ , defined as the product of the fraction of gas in each primordial object that is converted into stars ( $f_{\star}^{III}$ ), the number of PPSNe per unit mass of metal-free stars formed ( $\mathcal{N}^{\pm}$ ), the average kinetic energy per supernova ( $\mathcal{E}_{\text{kin}}$ ), and the fraction of the total kinetic energy channeled into the resulting galaxy outflow ( $f_{\text{wind}}$ ).

Here we focus on the later stage of metal-free star formation. Note that this is fundamentally different than star formation taking place in very small “minihalos” at redshifts  $\approx 25$ , which depends sensitively on the presence of initial  $H_2$  (e.g. O’Shea et al. 2005). In small objects, molecular hydrogen is easily photodissociated by 11.2-13.6 eV photons, to which the universe is otherwise transparent. This means that the emission from the first stars quickly destroyed all avenues for cooling by molecular line emission (Dekel & Rees 1987; Haiman, Rees, & Loeb 1997; Ciardi, Ferrara, & Abel 2000), which quickly raised the minimum virial temperature necessary to cool effectively to approximately  $10^4$  K. Thus the majority of primordial star formation is likely to have occurred in objects above this limit, who form their own  $H_2$  at high densities and are largely impervious to the photodissociating background (Oh & Haiman 2002).

Incorporating outflows into a detailed analytical model of such “primordial galaxies” leads to the approximate relation that, by mass, the fraction of the total star formation in metal-free stars at  $z = 4$  is

$$F_{\star}^{III}(z = 4) \sim 10^{-5}(\mathcal{E}_g^{III})^{-1}, \quad (5.1)$$

where, as above,  $\mathcal{E}^{\pm}$  is in units of  $10^{51}$  ergs per  $M_{\odot}$  of gas (see Figure 3 of SSF03 for details). Extrapolating the results in SSF03 to  $z = 0$  gives

$$F_{\star}^{III}(z = 0) \sim 10^{-5.5}(\mathcal{E}_g^{III})^{-1}. \quad (5.2)$$

These fractions can be related to the underlying population of stars by adopting fiducial values of  $f_{\star}^{III} = 0.1$  for the star formation efficiency, which is consistent with the observed star formation rate density at intermediate and high redshifts (Scannapieco, Ferrara, & Madau 2002), and  $f_w = 0.3$  for the wind efficiency, which is consistent with the dwarf galaxy outflow simulations of Mori, Ferrara, & Madau (2002). Finally, we assume that 1 pair-production SN occurs per 1000 solar masses of metal free stars. This gives  $F_{\star}^{III}$

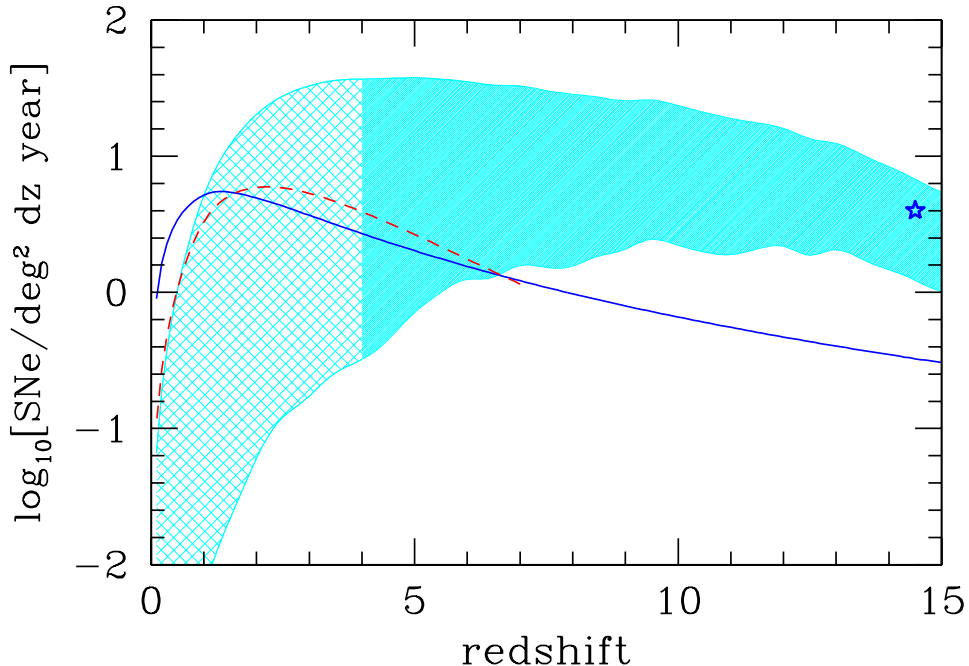


FIGURE 4. Number of PPSNe per square degree per unit redshift per year for a wide range of models. The solid and dashed curves assume Pop III star formation rate densities of  $0.001 M_{\odot} \text{ yr}^{-1} \text{ Mpc}^{-3}$  and 1% of the observed star formation rate density, respectively. The shaded region covers the range of metal-free star formation rate density models considered in SSF03, with the weakest feedback model ( $\mathcal{E}_g^{\text{III}} = 10^{-4}$ ) defining the upper end, and the strongest feedback model ( $\mathcal{E}_g^{\text{III}} = 10^{-2.5}$ ) defining the lower end. An extrapolation of these star formation rate densities to  $z = 0$  leads to the crosshatched region. In all SSF03 models the highest rates occur at redshifts  $\leq 10$ . Finally, the starred point is the  $z = 15$  estimate by Weinmann & Lilly (2005).

values of  $0.3(\mathcal{E}_{\text{kin}})^{-1}$  at  $z = 4$  and  $0.1(\mathcal{E}_{\text{kin}})^{-1}$  at  $z = 0$ , respectively. Or, in other words, for typical energies of  $30 \times 10^{51}$  ergs per PPSNe,  $\sim 1\%$  of the star formation at  $z = 4$  and  $\sim 0.3\%$  of the star formation at  $z = 0$  by mass should be in metal-free stars.

In Figure 4 we show estimates of the number of SNe per  $\text{deg}^2$  per  $dz$  *per year* over the wide range of models considered in SSF03, extrapolating to  $z = 0$ . In all cases we assume that 1 PPSN forms per 1000 solar masses of metal-free stars, and for comparison we show two simple estimates which we refer to further below. In the first simple model, we assume that metal-free star formation occurs at a constant rate density, which we take to be  $\rho^{\pm}(z)0.001 M_{\odot} \text{ yr}^{-1} \text{ Mpc}^{-3}$ , independent of redshift. In the second case, we assume that at all redshifts metal-free stars form at 1% of the observed total star formation rate density, which we model as  $\log_{10}[\rho_{\star}^{\text{obs}}(z)/M_{\odot} \text{ yr}^{-1} \text{ Mpc}^{-3}] = -2.1 + 3.9 \log_{10}(1+z) - 3.0 [\log_{10}(1+z)]^2$ , a simple fit to the most recent measurements (Giavalisco et al. 2004; Bouwens et al. 2004). For both star formation models we again assume that 1 pair-production SN occurs per 1000 solar masses of metal free stars.

Note that for the full range of models in Figure 4, metal-free star formation naturally occurs in the smallest galaxies, which are just large enough to overcome the thermal pressure of the ionized IGM, but small enough not to be clustered near areas of previous star formation (SSF03). In our adopted cosmology, for a temperature of  $10^4 \text{ K}$ , the minimum virial mass is  $3 \times 10^9 (1+z)^{-3/2} M_{\odot}$  with a corresponding gas mass of

$5 \times 10^8 (1+z)^{-3/2} M_\odot$ . This means the total stellar mass of primordial objects is likely to be around  $M_\star \approx 10^8 M_\odot (1+z)^{-3/2}$ , many orders of magnitude below  $L_\star$  galaxies. Thus in general blank-field surveys should be the best method for searching for PPSNe, as catalogs of likely host galaxies would be extremely difficult to construct.

Nevertheless, as VMS shine so brightly, a direct search for primordial host galaxies is not a hopeless endeavor. In particular the lack of dust in these objects and the large number of ionizing photons from massive metal-free stars leads naturally to a greatly enhanced Lyman alpha luminosity. Following SSF03 this can be estimated as

$$L_\alpha = c_L (1 - f_{\text{esc}}) Q(H) M_\star, \quad (5.3)$$

where  $c_L \equiv 1.04 \times 10^{-11}$  ergs,  $f_{\text{esc}}$  is the escape fraction of ionizing photons from the galaxy, which is likely to be  $\lesssim 0.2$  (see Ciardi, Bianchi, & Ferrara 2002 and references therein), and the ionizing photon rate  $Q(H)$  can be estimated as  $\approx 10^{48} \text{ s}^{-1} M_\odot^{-1}$  (Schaerer 2002). This gives a value of  $L_\alpha \sim 10^{45} (1+z)^{-3/2} \text{ ergs s}^{-1}$  which, if observed in a typical 1000 Å wide broad band corresponds to an absolute AB mag  $\sim -23 + 3.8 \log(1+z)$ , much brighter than the PPSNe themselves. However this flux would be spread out over many pixels and be more difficult to observe against the sky than the point-like PPSNe emission. For further details on the detectability of metal-free stars through Lyman-alpha observations, the reader is referred to SSF03.

## 6. Pair-Production Supernovae in Cosmological Surveys

From the models developed above, it is relatively straightforward to relate the star formation history of VMS to the resulting number of observable pair-production supernova. In this section and below we adopt cosmological parameters of  $h = 0.7$ ,  $\Omega_m = 0.3$ ,  $\Omega_\Lambda = 0.7$ , and  $\Omega_b = 0.045$ , where  $h$  is the Hubble constant in units of  $100 \text{ km s}^{-1}$  and  $\Omega_m$ ,  $\Omega_\Lambda$ , and  $\Omega_b$  are the total matter, vacuum, and baryonic densities in units of the critical density (e.g. Spergel et al. 2003).

Here we focus on three PPSN light curves, which bracket the range of possibilities: the faintest of all our models, 150-W, in which there is neither significant dredge-up nor  $^{56}\text{Ni}$  production; an intermediate model, 200-I, in which some dredge-up occurred, but  $5.1 M_\odot$  of  $^{56}\text{Ni}$  were formed; and the model with the brightest lightcurves, 250-S, in which substantial dredge-up leads to an enormous initial radius of over 20 A.U., and the production of  $24.5 M_\odot$  of  $^{56}\text{Ni}$  causes an extended late-time period of high luminosity. Note that we do not address the possibility of extinction by dust, which amounts to assuming that pristine regions remain dust-free through the lifetime of the very massive PPSN progenitor stars.

For any given PPSN model, we can calculate  $t(\lambda, F_\nu^{\text{min}}, z)$  the total time the observed flux at the wavelength  $\lambda$  from a SN at the redshift  $z$  is greater than the magnitude limit associated with the specific flux  $F_\nu^{\text{min}}$ . The total number of PPSNe shining at any given time with fluxes above  $F_\nu^{\text{min}}$ , per square degree per unit redshift is then given by the product of the volume element, the (time-dilated) PPSN rate density, and the time a given PPSN is visible, that is

$$\frac{dN_{\text{deg}^2}}{dz}(\lambda, F_\nu^{\text{min}}, z) = [r(z) \sin(1\text{deg})]^2 \frac{dr}{dz} \frac{\rho^\pm(z)}{1+z} t(\lambda, F_\nu^{\text{min}}, z), \quad (6.1)$$

where the rate density  $\rho^\pm(z)$  is the number of PPSNe per unit time per comoving volume as a function of redshift.

The resulting observed PPSNe counts for these models are given in Figure 5 for two

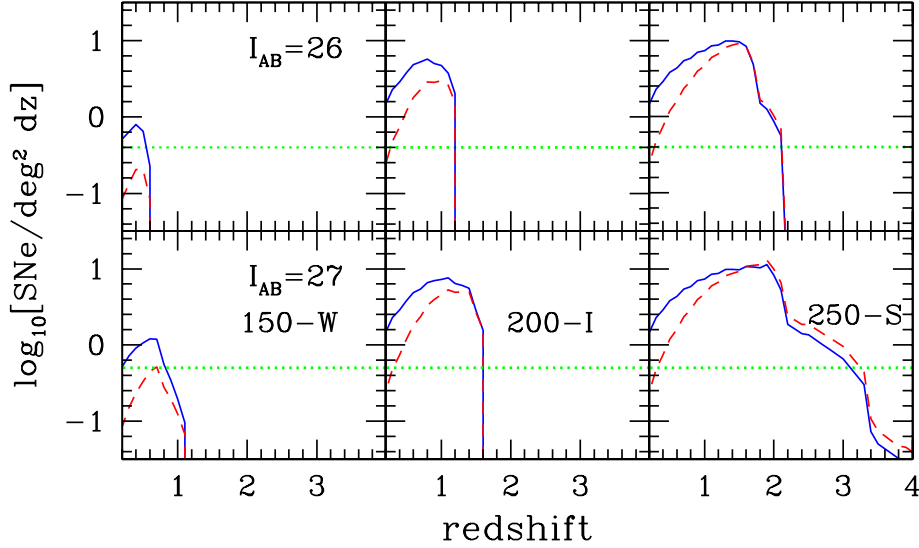


FIGURE 5. Number of PPSNe per square degree per unit redshift above a given I-band magnitude, assuming  $0.001 \text{ M}_{\odot} \text{ yr}^{-1} \text{ Mpc}^{-3}$  (solid lines) or 1% of the observed star formation rate density (dashed lines). The  $I_{AB} = 26$  cut taken in the upper rows approximately corresponds to the magnitude limit of the Institute for Astronomy Deep Survey which covered  $2.5 \text{ deg}^2$  (as shown by the dotted lines) from September 2001 to April 2002. The  $I_{AB} = 27$  limit in the bottom panel corresponds to that of the ongoing COSMOS survey, which will survey an area of  $2 \text{ deg}^2$  (again indicated by the dotted lines). Note however, that the COSMOS survey itself is primarily focused on large-scale structure issues and will not be able to find PPSNe, as each pointing is visited only once.

limiting magnitudes. In the upper panels, we take a  $I_{AB} = 26$  magnitude limit, appropriate for the Institute for Astronomy (IfA) Deep Survey (Barris et al. 2004), a ground-based survey that covered a total of  $2.5 \text{ deg}^2$  from September 2001 to April 2002. As we are focused on lower-redshift observations, we only plot estimated counts for the two simple rate density models described in §5, rather than the more detailed (but higher redshift) SSF03 models.

From this figure we see that existing data sets, if properly analyzed, are easily able to place useful constraints on PPSN formation at low redshifts. Given a typical model like 200-I for example, the already realized IfA survey can be used to place a constraint of  $\lesssim 1\%$  of the total star formation rate density out to a redshift  $\approx 1$ . Similarly, extreme models such as 250-S can be probed out to redshifts  $\approx 2$ , all within the context of a recent SN search driven by completely different science goals. Note however that these limits are strongly dependent on significant mixing in the SN progenitor or the production of  $^{56}\text{Ni}$ , and thus models such as 150-W remain largely unconstrained by the IfA survey.

In the bottom panels of Figure 5 we consider a limiting magnitude of  $I_{AB} = 27$ , appropriate for the COSMOS survey<sup>†</sup>, a project that covers  $2 \text{ deg}^2$  using the *Advanced Camera for Surveys* on HST. Raising the limiting magnitude from  $I_{AB} = 26$  to  $I_{AB} = 27$

<sup>†</sup> see <http://www.astro.caltech.edu/~cosmos/>

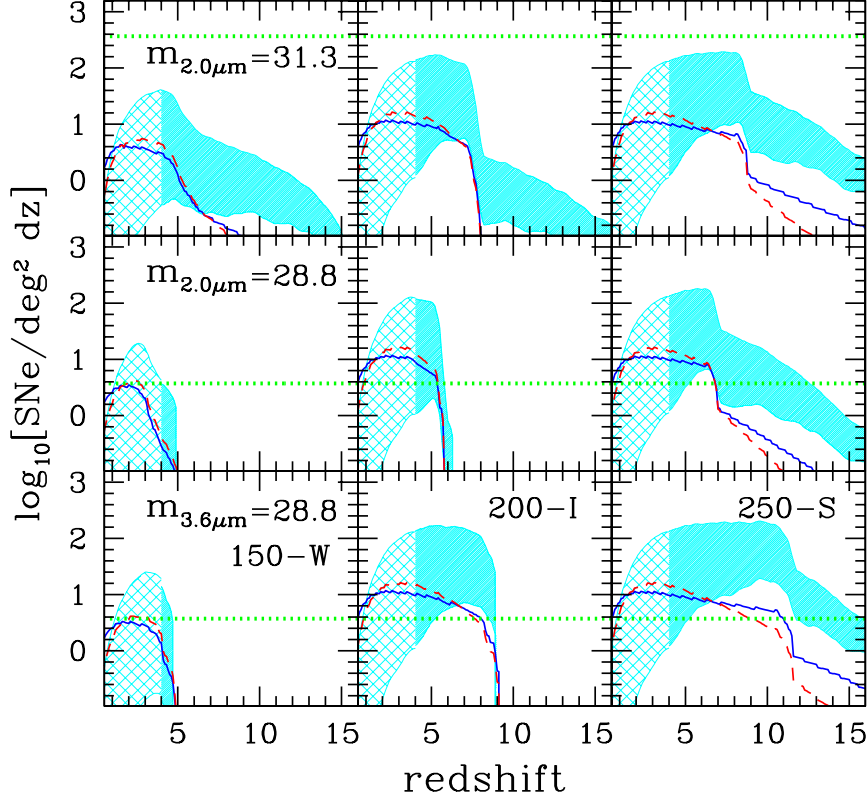


FIGURE 6. Number of PPSNe per square degree per unit redshift above a fixed AB magnitude, with limits appropriate for three possible surveys with the James Webb Space Telescope. Curves are as in Figure 5, while the shaded regions are predictions from the full range of SSF03 models described in §5. *Top*: The 31.1 AB magnitude limit taken in these panels corresponds to the  $10\sigma$  detection limit for a  $10^6$  sec integration with at  $2\mu\text{m}$  with the NIRCcam instrument. While this would be able to probe SN extremely deeply, it would only cover a  $9.8\text{ arcmin}^2$  patch of the sky, corresponding to the dotted lines. No detections would be expected in this small area. *Center*: The 28.8 AB magnitude  $2\mu\text{m}$  limit taken in these panels corresponds to the  $10\sigma$  detection limit for a  $10^4$  second integration with NIRCcam. In  $10^6$  seconds, such measurements could be taken at roughly 100 pointings, covering a  $0.3\text{ deg}^2$  area, corresponding to the dotted lines. In this case  $\sim 10$  PPSNe like 150W or 200I would be detectable out to  $z \approx 6$ , while up to  $\sim 30$  PPSNe like 250S would be detectable out to  $z \approx 10$ . *Bottom*: The 28.8 AB magnitude  $3.6\mu$  limit taken in these panels again corresponds to  $10\sigma$  detections for a  $10^4$  second NIRCcam integration. Moving to a longer wavelength results in a significant boost to both the number of detectable PPSNe and the maximum redshift at which they can be observed.

has the primary effect of extending the sensitivity out to slightly higher redshifts. This pushes the probed range from  $z \lesssim 1$  to  $z \lesssim 1.5$  in the 200-I case and from  $z \lesssim 2$  to  $z \lesssim 3$  in the 250-S case. Again this is all in the context of an ongoing survey. Even with this fainter limiting magnitude, however, low-luminosity PPSNe like 150-W are extremely difficult to find, and remain largely unconstrained.

This shortcoming is easily overcome by moving to NIR wavelengths. In Figure 6 we present for the first time similar limits computed for the James Webb Space Telescope

(JWST), using both the simple models PopIII SFR density models shown in Figure 5 as well as the full range of more detailed models computed in SSF03. With JWST,  $dN_{\text{deg}^2}/dz$  is dramatically increased with respect to ground-based searches. This is due to the fact that for the majority of their lifetimes, the effective temperatures of PPSNe are just above the  $\approx 10^{3.8}K$  recombination temperature of hydrogen, which corresponds to a peak black-body wavelength  $\approx 8000 \text{ \AA}$ . This means that for all but the lowest redshifts, the majority of the emitted light is shifted substantially redward of the I-band, which is centered at  $9000 \text{ \AA}$ . Given the sensitivities described in Gardner et al. (2006), a  $10^6$  second NIRCcam at  $2.0\mu$  integration would be able to see a PPSN out to  $z \approx 15$ .

In fact, NIRCcam will be so sensitive that using it to perform extremely long integrations will *not* be the best way to search for PPSNe. Rather, the key issue will be covering enough area to find them at the rates expected from theoretical models. As a single NIRCcam pointing only covers 9.8 square arcminutes, any individual such field is not likely to host a PPSN, even at such very faint magnitudes. Rather a much more efficient method is to carry out a survey composed of roughly 100 pointings, each with a  $10^4$  second integration time. In this case,  $\sim 10$  PPSNe like 150W or 200I would be detectable out to  $z \approx 6$ , while up to  $\sim 30$  PPSNe like 250S would be detectable out to  $z \approx 10$ . Furthermore, moving to slightly longer wavelengths, increases the high-redshift sensitivity much in the same way as carrying out longer integrations at a fixed band. Thus the expected number of PPSNe/deg<sup>2</sup>/dz above an AB magnitude limit of 28.8 at  $3.6\mu\text{m}$  is comparable to the number of PPSNe/deg<sup>2</sup>/dz above an AB magnitude limit of 31.3 at  $2.0\mu\text{m}$ .

Taken together, these results imply that the optimal strategy for searching for PPSNe with JWST will be to carry out a 2 or 3 band NIRCcam survey (to obtain color information on these objects), with an emphasis on longer wavelengths (to boost sensitivity), made up of  $\approx 100$  pointings with moderate integration times (to maximize sky coverage). Finally as most of the features in PPSNe lightcurves are on the 30-100 day scale, this field should be revisited roughly once per 30 days  $\times (1+z) \approx 1$  year, on three occasions. Although this would require about 1-2 weeks of dedicated time each year, clearly this program could be carried out in the context of a more general deep-field study, such as the present Supernova Cosmology Project in the context of the Great Observatories Origins Deep Survey with HST.

## 7. Modeling the Galactic Descendants of Metal-Free Stars

A secondary method of searching for PPSN is the detection of their nucleosynthetic products in present day stars. However, interpretation of these abundances is complicated by the fact that searches for metal-poor stars are limited to the Galactic halo, where dust extinction and crowding are minimal. In fact, these analyses have already provided a number intriguing constraints on the enrichment history of the halo (Freeman & Bland-Hawthorn 2002; Beers & Christlieb 2005), including uncovering the presence of extremely heavy-element deficient stars (Christlieb et al. 2002; Frebel et al. 2005). Yet, it is still unclear how the observed population of halo stars is related to PopIII star formation (White & Springel 2000; Diemand, Madau, & Moore 2005).

To quantify this, in Scannapieco et al. (2006), we combined a high-resolution N-body simulation of the formation of the Milky-Way with a semi-analytical model of metal enrichment similar to that in SSF03. Our N-body simulation was carried out with the GCD+ code (Kawata & Gibson 2003a), and it used a multi-resolution technique (Kawata & Gibson 2003b) to achieve high-resolution within a 1 Mpc radius, while the outer regions exerting tidal forces were handled with lower resolution. In the high-resolution region, the dark matter particle mass was  $M_{\text{vir}} = 7.8 \times 10^5 M_{\odot}$ , compared to the final virial

mass of  $M_{\text{vir}} = 7.7 \times 10^{11} M_{\odot}$ . The simulation data was output every 0.11 Gyr, and at each output, we use a friend-of-friends (FOF) group finder to identify the virialized DM halos, with a linking parameter of  $b = 0.2$ . As in §5 we then assumed star formation to occur in all halos with virial temperatures above the atomic cooling limit of  $10^4$  K, which corresponds to a minimum mass of  $M_{\text{min}} \equiv 3.0 \times 10^9 (1+z)^{-3/2} M_{\odot}$ . This means that even at a very high redshift of 20, all the halos relevant to our study contained at least 50 particles, and are well-identified by a FOF group finder.

Our next step was to use this accretion history to identify two types of objects: i) halos that collapsed out of primordial gas, which we identified as PopIII objects containing “the first stars,” and ii) halos that collapsed from gas that has been enriched purely by PopIII objects, which we identified as second-generation objects containing “the second stars.” Following our approach in SSF03, we adopted a model of outflows as spherical shells expanding into the Hubble flow (Ostriker & McKee 1988) for both PopIII and PopII/I objects. These shells were assumed to be driven only by the internal hot gas pressure and decelerated by accreting material and gravitational drag. The evolution of each such bubble was then completely determined by the mechanical energy imparted to the outflow. In particular the only difference between PopIII and PopII/I outflows arises from the energy input per unit gas mass,”  $\mathcal{E}_g^{\text{III,II}}$ .

In the PopII/I case, we calculated this assuming that 10% of the gas was converted into stars, that  $10^{51}$  ergs of kinetic energy input  $300 M_{\odot}$  of stars formed, and we assumed an overall wind efficiency fit to results of Mori, Ferrara, & Madau (2002) and Ferrara, Pettini, & Shchekinov (2000). In the PopIII case, on the other hand, as there are no direct constraints, we varied  $\mathcal{E}_g^{\text{III}}$  over a large range as in §5. Finally, when outflows slowed down to the IGM sound speed, we assumed they fragmented and let them expand with the Hubble flow. For further details, the reader is referred to Scannapieco et al. (2006).

## 8. The Spatial Distribution of the Galactic Descendants of Metal-Free Stars

Figure 7 demonstrates the positions of the first and second stars at different redshifts in the Lagrangian model with  $\mathcal{E}_g^{\text{III}} = 10^{-2}$ . At early times ( $z = 9.84$ ), the first stars form close to the central density peak of the progenitor galaxy, due to the higher density peaks in this region. Second stars form in the halo in the neighborhood of first stars, because they condense from gas that is enriched by the material from the explosions of the first stars. At a later time ( $z = 6.02$ ), new first stars are still forming, but now on the outer regions of the progenitor galaxy, because they are not yet affected by winds from the central region. The formation of the first and second stars is complete around  $z = 3$ , at which time the full region is enriched with metals. Also at this redshift, first and second stars start to be accreted into the assembling Galactic halo. This assembly is almost complete by  $z = 1$ , and thus the distribution at this redshift is similar to that at  $z = 0$ .

In Figure 8 we plot the radial mass density of first and second stars, as compared to the dark matter distribution in our simulation. In computing these masses, we assume that 10% of the gas mass in each halo is converted into stars and we intentionally make no attempt to account for mass loss due to stellar evolution. Furthermore, we plot only out to 250 kpc, which is 1/4 the size of the high-resolution region. Here we see that the density profiles of first and second stars are similar to the total dark matter density profile, although the second stars have a slightly shallower slope. As a result, the density of first stars at the center is 100 times higher than at the 8 kpc orbital radius of the

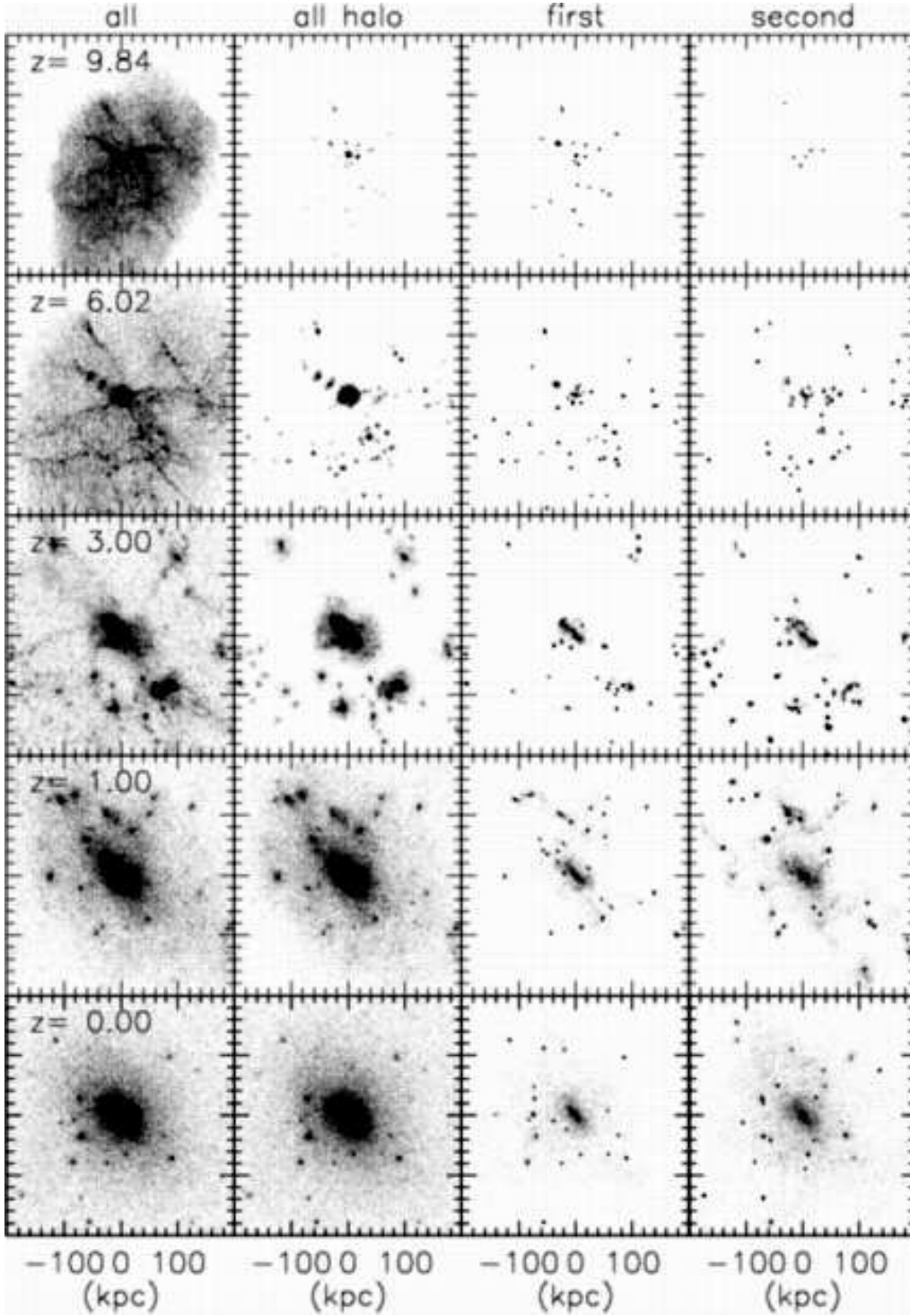


FIGURE 7. Distributions of first and second stars (3rd and 4th columns) in a  $200 \text{ proper kpc}^3$  region, at various redshifts, for a model with  $\epsilon_g^{III} = 10^{-2}$ . For comparison, the 1st and 2nd columns show all the particles and all the particles that were ever within a halo with a virial temperature above the atomic cooling limit, respectively.

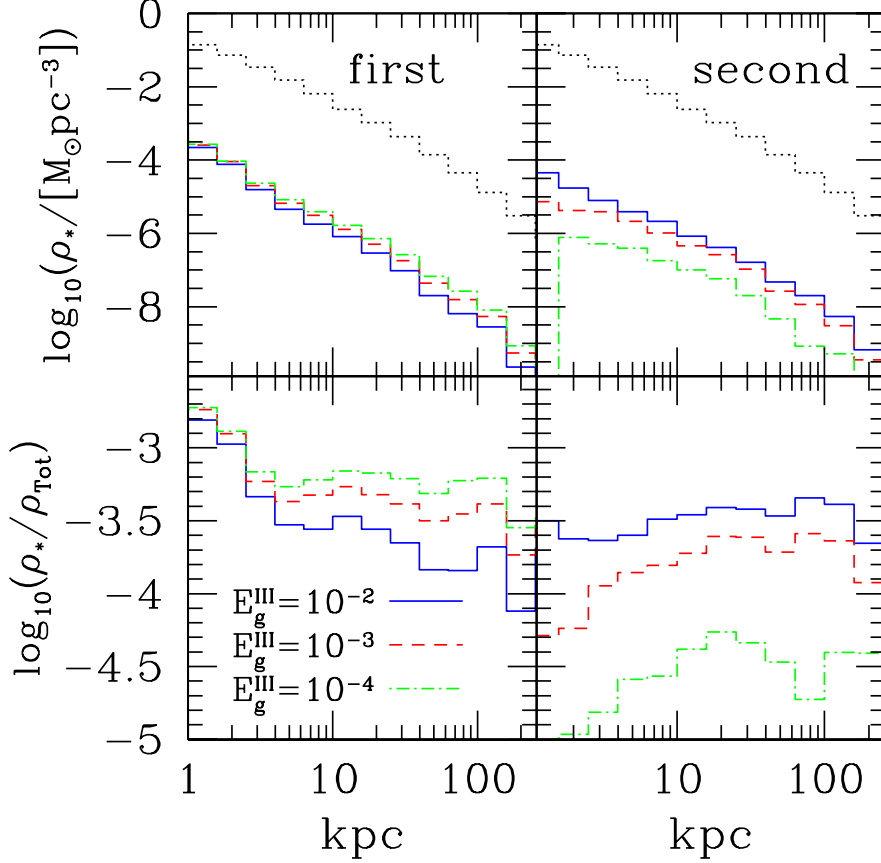


FIGURE 8. Radial profile of first (left column) and second stars (right column) at  $z = 0$ . In the top row, the dotted lines give the overall dark matter profile of the galaxy, which is compared with the radial density of first and second stars in models with  $\mathcal{E}_g^{III} = 10^{-2}$  (solid),  $\mathcal{E}_g^{III} = 10^{-3}$  (short-dashed), and  $\mathcal{E}_g^{III} = 10^{-4}$  (dot-dashed). The lower row shows the fraction of the total density in first and second stars, with symbols as in the upper panels. Note that this plot does not include any mass loss due to stellar evolution.

sun. However, the important number for developing observational strategies for finding the first stars is their relative density with respect to the field stars. While this is not directly computed in our simulation, the lower panels of Figure 8 show the local mass density of stars normalized by the local density of dark matter.

Amazingly, the mass fraction contained in the first stars varies only very weakly with radius. Moving from 1 to 100 kpc in the  $\mathcal{E}_g^{III} = 10^{-4}$  model, for example, the fraction of the mass in first stars decreases only by a factor  $\approx 4$ . Furthermore, increasing the efficiency of PopIII winds to  $\mathcal{E}_g^{III} = 10^{-2}$  has the effect of decreasing the fraction of first stars without strongly affecting their radial distribution.

This is both good and bad news for PPSNe models. First of all it means that observations of metal-poor stars in the Galactic halo should be taken as directly constraining the properties of primordial objects. Thus the lack of metal-free stars observed in the halo is likely to imply a real lower mass limit in the metal free initial mass function (IMF) of at

least  $0.8 M_{\odot}$ , the mass of a low-metallicity star with a lifetime comparable to the Hubble time (Fagotto et al. 1994). In fact the  $\sim 10^{-6} M_{\odot} \text{ pc}^{-3}$  value for PopIII stars in the solar neighborhood we compute is so high as compared to the observed stellar mass density of  $5 \times 10^{-5} M_{\odot} \text{ pc}^{-3}$  (Preston, Sheckman, & Beers 1991), that several primordial  $0.8 M_{\odot}$  stars would have been observed even if  $f_*^{III}$  were over an order of magnitude lower than the 0.1 value we used to normalize our approach. This lends strong support to models of metal free stars as biased to high masses.

On the other hand, it also means that the abundances we see in very metal poor stars should be taken to constrain elements produced in the first stars. In particular, if a large fraction of PopIII star formation resulted in PPSNe, then the strong odd-even effect discussed in §2 should be measurable in a subset of stars with  $[\text{Fe}/\text{H}] \leq -2$ . To date these measurements have failed to uncover this signal. As discussed in Tumlinson (2006), this does not rule out the presence of PPSNe, but it does argue strongly that a significant number of PopIII stars ended their lives as more usual core-collapse supernovae.

## 9. Summary

Theoretically, PPSNe are the simplest of all supernovae. Driven by a well-understood dynamical instability, and leading to complete stellar disruption, they are the uniquely calculable result of nonrotating stars than end their lives in the  $140 - 260 M_{\odot}$  mass range (Heger & Woosley 2002). The issue is only when and where such stars existed. In the present, enriched, universe the observed upper mass limit of forming stars, and the rate of mass loss in O stars argue strongly against these objects. However, in the primordial high-redshift universe things are likely to have been very different. The typical fragmentation mass under these conditions is  $\approx 1000 M_{\odot}$  and stellar winds, at least of the line driven type observed today, are expected to be negligible. This raises the real possibility that in the metal-free universe a large fraction of stars generated PPSNe.

As metal-enrichment is an intrinsically local process that proceeds over an extended redshift range, at each redshift, pockets of metal-free star formation are naturally confined to the lowest-mass galaxies, which are small enough not to be clustered near areas of previous star formation. As such faint galaxies are difficult to detect and even more difficult to confirm as metal-free, the hosts of PPSNe could easily be lurking at the limits of present-day galaxy surveys.

In S05 we showed that the most important factors for modeling PPSNe lightcurves are the mass of the progenitor star and the efficiency of dredge-up of carbon from the core into the envelope. In general, increasing the mass leads to greater  $^{56}\text{Ni}$  production, which boosts the late time SN luminosity. Mixing, on the other hand, has two major effects: it leads to a red giant phase that increases the early-time SN luminosity and it decreases the mass of the He core, consequently leading to a somewhat smaller mass of  $^{56}\text{Ni}$ . Despite these uncertainties, PPSNe in general can be characterized by: (1) peak magnitudes that are brighter than Type II SNe and comparable or slightly brighter than typical SNe Type Ia; (2) very long decay times  $\sim 1$  year, which result from the large initial radii and large masses of material involved in the explosion; and (3) the presence of hydrogen lines, which are caused by the outer envelope.

The S05 lightcurves also allowed us to calculate the number of PPSNe detectable in current and planned supernova searches. Here the long lifetimes help to keep a substantial number of PPSNe visible at any given time, meaning that ongoing SN searches should be able to limit the contribution of VMS to  $\lesssim 1\%$  of the total star formation rate density out to a redshift of 2, unless both mixing and  $^{56}\text{Ni}$  production are absent for all PPSNe. Such constraints already place meaningful limits on the cosmological models.

The impact of future NIR searches is even more promising, as the majority of the PPSN light is emitted at restframe wavelengths longward of  $\approx 8000 \text{ \AA}$ . In particular JWST surveys with NIRCcam have the potential to place fantastic constraints on PPSNe out to  $z \approx 10$ . In this case the best approach will be a  $\approx 0.3 \text{ deg}^2$  survey made up of  $\approx 100$  NIRCcam pointings with  $\approx 10^4$  sec integrations in two or three bands, with emphasis on the redder colors. Furthermore this field should be revisited with a cadence of roughly once per year on three occasions. Although this would require about 1-2 weeks of dedicated time each year, clearly this program could be carried out in the context of a more general deep field study, with a much broader set of science goals.

Closer to home, we have also studied the final distribution of the elements synthesized in primordial stars. Despite the large uncertainties involved, all models generically predict significant PopIII star formation in what is now the Galactic halo. Thus, if they have sufficiently long lifetimes, a significant number of stars formed in initially primordial star clusters should be found in ongoing surveys for metal-poor halo stars. This is both good and bad news for PPSNe models. While it implies a real lower mass limit for the PopIII IMF of at least  $0.8 M_{\odot}$ , it also suggests that the lack of an odd-even effect in the observed abundance ratios of metal-poor stars should be taken as evidence that a significant number of PopIII stars ended their lives as more usual core-collapse supernovae.

However, definitive limits on PPSNe will only come from space based NIR surveys. If they result in detections, they will open a new window on star formation and the history of cosmological chemical enrichment. If they result in upper limits, they will place exquisite constraints on the presence of PPSN forming in primordial environments above the atomic cooling limit, but leave open the question of their formation in the first “minihalos” collapsing at extremely high redshift. While this would remain a possibility, the absence of detections from space-based searches would limit PPSN to the most remote and undetectable corner of the universe. Undaunted theorists might still wish to discuss them in workshops on the deepest depths of the cosmological dark ages. Observers may be reminded that “he who wishes to lie, should put the evidence far away” (Livio 2006).

I would like to thank my collaborators Chris Brook, Andrea Ferrara, Brad Gibson, Alexander Heger, Daisuke Kawata, Piero Madau, Raffaella Schneider, and Stan Woosley, for allowing me to present the results of our work together here. I am also thankful to Jonathan Gardner, for providing detailed information on the planned capabilities of the James Webb Space Telescope. Finally, I would like to thank Mario Livio, Massimo Stiavelli, and the other members of the organizing committee as well as the many excellent speakers for a fun and informative symposium.

## REFERENCES

- ABEL, T., BRYAN, G. L. & NORMAN, M. L. 2002 The formation of the first star in the universe *Science* **295**, 93–98
- BARKAT, Z., RAKAVY, G. & SACK, N. 1967 Dynamics of supernova explosion resulting from pair formation *Phys. Rev. Lett.* **18**, 379–381
- BARBON, R., CIATTI, F., ROSINO, L., ORTOLANI, S. & RAFANELLI, P. 1982 Spectra and light curves of three recent supernovae *Astron. & Astrophys.* **116**, 43–53
- BARRIS, B. J. ET AL. 2004 Twenty-three high-redshift supernovae from the institute for astronomy deep survey: doubling the supernova sample at  $z \geq 0.7$  *Astrophys. J.* **602**, 571–594
- BEERS, T. C. & CHRISTLIEB, N. 2002 The discovery and analysis of very metal-poor stars in the Galaxy *Ann. Rev. of Astron. & Astrophys.* **43**, 521–580
- BOND, J. R., ARNETT, W. D. & CARR, B. J. 1984 The evolution and fate of very massive objects *Astrophys. J.* **280**, 825–847

- BOUWENS, R. ET AL. 2004 Galaxies at  $z \sim 7-8$ :  $z850$ -Dropouts in the Hubble Ultra Deep Field *Astrophys. J. Lett.* **616**, 79–82
- CAPPELLARO, E., MAZZALI, P. A., BENETTI, S., DANZIGER, I. J., TURATTO, M., DELLA VALLE, M. & PATAT, F. 1997 SN IA light curves and radioactive decay *Astron. & Astrophys.* **328**, 203–210
- CATCHPOLE, R. M., ET AL. 1988 Spectroscopic and photometric observations of SN 1987A. III - Days 135 to 260 *Mon. Not. of the Royal Astron. Soc.* **231**, 75–89
- CIARDI, B., BIANCHI, S. & FERRARA, A. 2002 Lyman continuum escape from an inhomogeneous interstellar medium *Mon. Not. of the Royal Astron. Soc.* **331**, 463–473
- CIARDI, B., FERRARA, A. & ABEL, T. 2000 Intergalactic  $H_2$  photodissociation and the soft ultraviolet background produced by Population III objects *Astrophys. J.* **533**, 594–600
- CHRISTLIEB, N. ET AL. 2002 A stellar relic from the early Milky Way *Nature*, **419**, 904–906
- DE VAUCOULEURS, G., DE VAUCOULEURS, A., BUTA, R., ABELS, H. D. & HEWITT, A. V. 1981 The bright supernova 1979c in M100 *Pubs. of the Astron. Soc. of the Pacific* **93**, 36–44
- DEKEL, A. & REES, M. J. 1987 Physical mechanisms for biased galaxy formation *Nature* **326**, 455–462
- DIEMAND, J., MADAU, P. & MOORE, B. 2005 The distribution and kinematics of early high- $\sigma$  peaks in present-day haloes: implications for rare objects and old stellar populations *Mon. Not. of the Royal Astron. Soc.* **364**, 367–383
- EASTMAN, R. G., WOOSLEY, S. E., WEAVER, T. A., & PINTO, P. A. 1993 The theoretical light curve and spectral evolution of type II supernovae *Bull. Am. Astron. Soc.* **25**, 836.
- EASTMAN, R. G., WOOSLEY, S. E., WEAVER, T. A., & PINTO, P. A. 1994 Theoretical light curve of a Type 2p supernova *Astrophys. J.* **430**, 300–310
- ELMHANDI, A. ET AL. 2003 Photometry and spectroscopy of the Type IIP SN 1999em from outburst to dust formation *Mon. Not. of the Royal Astron. Soc.* **338**, 939–956
- FAGOTTO, F., BRESSAN, A., BERTELLI, G. & CHIOSI, C. 1994, Evolutionary sequences of stellar models with new radiative opacities. III.  $Z=0.0004$  and  $Z=0.05$  *Astron. & Astrophys. Suppl.* **104**, 365–376
- FERRARA, A., PETTINI, M. & SHCHEKINOV, Y. 2000 Mixing metals in the early Universe *Mon. Not. of the Royal Astron. Soc.* **319**, 539–548
- FIGER, D. 2005 An upper limit to the masses of stars *Nature* **434**, 192–194
- FRALEY, G. S. 1968 Supernovae explosions induced by pair-production instability *Astrophys. & Space Sci.* **2**, 96–114
- FREBEL, A. ET AL. 2005 A stellar relic from the early Milky Way *Nature*, **434**, 871–873
- FREEMAN, K. & BLAND-HAWTHORN, J. 2002 The new Galaxy: signatures of its formation *Ann. Rev. of Astron. & Astrophys.* **40**, 487–537
- FRYER, C., L., WOOSLEY, S. E. & HEGER, A. 2001 Pair-instability supernovae, gravity waves, and gamma-ray transients *Astrophys. J.* **550**, 372–382
- GARDNER, J. P. ET AL. 2006, The James Webb Space Telescope SPACE SCIENCE REVIEWS, in press (astro-ph/0606175).
- GIAVALISCO, M. ET AL. 2004 The rest-frame ultraviolet luminosity density of star-forming galaxies at redshifts  $z > 3.5$  *Astrophys. J. Lett.* **600**, 103–106
- HAIMAN, Z., REES, M. J. & LOEB A. 1997 Destruction of molecular hydrogen during cosmological reionization *Astrophys. J.* **476**, 458–463
- HAMUY, M., SUNTZEFF, N. B., GONZALEZ, R., & MARTIN, G. 1988, *Astron. J.*, **95**, 63–83
- HEGER, A. & WOOSLEY, S. E. 2002 The nucleosynthetic signature of Population III *Astrophys. J.* **567**, 532–543
- KAWATA, D. & GIBSON, B. K. 2003a GCD+: a new chemodynamical approach to modelling supernovae and chemical enrichment in elliptical galaxies *Mon. Not. of the Royal Astron. Soc.* **340**, 908–922
- KAWATA, D. & GIBSON, B. K. 2003b Multiwavelength cosmological simulations of elliptical galaxies *Mon. Not. of the Royal Astron. Soc.* **346**, 135–152
- KUDRITZKI, R. 2000 Wind models and ionizing fluxes of massive stars at very low metallicity In *The First Stars. Proceedings of the MPA/ESO Workshop held at Garching, Germany, 4-6 August 1999* (eds. A. Weiss, T. Abel, & V. Hill) pp. 127–132 Springer
- KUDRITZKI, R. P. 2002 Line-driven winds, ionizing fluxes, and ultraviolet spectra of hot stars at extremely low metallicity. I. very massive O stars *Astrophys. J.* **577**, 389–408

- LIVIO, M. 2006 Free translation from Hebrew *Not so private communication*
- MORI, M., FERRARA, A. & MADAU, P. 2002 Early metal enrichment by pregalactic outflows. II. Three-dimensional simulations of blow-away *Astrophys. J.* **571**, 40–55
- NAKAMURA, F. & UMEMURA, M. 1990 On the mass of Population III stars *Astrophys. J.* **515**, 239–248
- O'EY, M. S. & CLARKE, C. J. 2005 Statistical confirmation of a stellar upper mass limit *Astrophys. J. Lett.* **620**, 43–46
- OH, S. P. & HAIMAN, Z. 2002 Second-generation objects in the Universe: radiative cooling and collapse of halos with virial temperatures above  $10^4$  K *Astrophys. J.* **569**, 558–572
- O'SHEA, ABEL, T., WHALEN, D. & NORMAN, M. L. 2005 Forming a primordial star in a relic III region *Astrophys. J. Lett.* **628**, 5
- OSTRIKER, J. P. & MCKEE, C. F. 1988 Astrophysical blastwaves *Rev. Mod. Phys.* **60**, 1–68
- PATAT, F., BENETTI, S., CAPPELLARO, E., DANZIGER, I. J., DELLA VALLE, M., MAZZALI, P. A., & TURATTO, M. 1996 The type IA supernova 1994D in NGC 4526: the early phases *Mon. Not. of the Royal Astron. Soc.* **278**, 111–124
- PRESTON, G. W., SHECTMAN, S. A., & BEERS, T. 1991 Detection of a galactic color gradient for blue horizontal-branch stars of the halo field and implications for the halo age and density distributions *Astrophys. J.* **375**, 121–147
- SCANNAPIECO, E., FERRARA, A., & MADAU, P. 2002 Early enrichment of the intergalactic medium and its feedback on galaxy formation *Astrophys. J.* **574**, 590–598
- SCANNAPIECO, E., SCHNEIDER, R. & FERRARA, A. 2003 The detectability of the first stars and their cluster enrichment signatures *Astrophys. J.* **589**, 35–52
- SCANNAPIECO, E., MADAU, P., WOOSLEY, S., HEGER, A., & FERRARA, A. 2005 The Detectability of Pair-Production Supernovae at  $z \lesssim 6$  *Astrophys. J.* **663**, 1031–1041
- SCANNAPIECO, E., KAWATA, D., BROOK, C. B., SCHNEIDER, R., FERRARA, A., & GIBSON, B. K. 2006 The spatial distribution of the Galactic first stars I: High-resolution N-body approach *Astrophys. J.* in press.
- SCHAEERER, D. 2002 On the properties of massive Population III stars and metal-free stellar populations *Astron. & Astrophys.* **382**, 28–42
- SCHNEIDER, R., FERRARA, A., NATARAJAN, P. & OMUKAI, K. 2002 First stars, very massive black holes, and metals *Astrophys. J.* **571**, 30–39
- SMITH, N. & OWOCKI, S. P. 2006 On the role of continuum-driven eruptions in the evolution of very massive stars and Population III stars *Astrophys. J. Lett.*, In press (astro-ph/0606174)
- SPERGEL, D. N., ET AL. 2003 First-Year Wilkinson Microwave Anisotropy Probe (WMAP) Observations: Determination of Cosmological Parameters *Astrophys. J. Supp.* **14**, 175–194
- TAN, J. C. & MCKEE, C. F. 2004 The formation of the first stars. I. mass infall rates, accretion disk structure, and protostellar evolution *Astrophys. J.* **603**, 383–400
- Chemical evolution in hierarchical models of cosmic structure. I. constraints on the early stellar initial mass function TURLINSON, J. 2006 *Astrophys. J.* **641**, 1–20
- VINK, J. S., DE KOTER, A., & LAMERS, H. J. G. L. M. 2001 Mass-loss predictions for O and B stars as a function of metallicity *Astro. & Astrophys.* **369**, 574–588
- WEAVER, T. A., ZIMMERMAN, G. B., & WOOSLEY, S. E. 1978 Presupernova evolution of massive stars *Astrophys. J.* **225**, 1021–1029
- WEAVER, T. A., & WOOSLEY, S. E. 1980, Evolution and explosion of massive stars In *Ninth Texas Symposium on Relativistic Astrophysics* pp. 335–357 New York Academy of Sciences,
- WEIDNER, C. & KROUPA, P. 2004 Evidence for a fundamental stellar upper mass limit from clustered star formation *Mon. Not. of the Royal Astron. Soc.* **348** 187–191
- WEINMANN, S. M. & LILLY, S. J. 2005 The number and observability of Population III supernovae at high redshifts *Astrophys. J.* **624** 526–531.
- WHITE, S. D. M., & SPRINGEL, V. 2000, In *The First Stars. Proceedings of the MPA/ESO Workshop held at Garching, Germany, 4-6 August 1999* (eds. A. Weiss, T. Abel, & V. Hill) pp. 327–335 Springer